

StablePDENet: Enhancing Stability of Operator Learning for Solving Differential Equations

Chutian Huang¹, Chang Ma^{*1}, Kaibo Wang¹, and Yang Xiang^{*1,2}

¹Department of Mathematics, The Hong Kong University of Science and Technology,
Clear Water Bay, Kowloon, Hong Kong

²Algorithms of Machine Learning and Autonomous Driving Research Lab, HKUST
Shenzhen-Hong Kong Collaborative Innovation Research Institute, Shenzhen, China

Abstract

Learning solution operators for differential equations with neural networks has shown great potential in scientific computing, but ensuring their stability under input perturbations remains a critical challenge. This paper presents a robust self-supervised neural operator framework that enhances stability through adversarial training while preserving accuracy. We formulate operator learning as a min-max optimization problem, where the model is trained against worst-case input perturbations to achieve consistent performance under both normal and adversarial conditions. We demonstrate that our method not only achieves good performance on standard inputs, but also maintains high fidelity under adversarial perturbed inputs. The results highlight the importance of stability-aware training in operator learning and provide a foundation for developing reliable neural PDE solvers in real-world applications, where input noise and uncertainties are inevitable.

Keywords: Neural operators, adversarial training, stability, self-supervised learning

1 Introduction

In recent years, neural network-based approaches have shown promising performance in addressing the forward and inverse problems of partial differential equations (PDEs) raised in science and engineering, including fluid dynamics, climate modeling, and molecular dynamics, materials mechanics, etc [1, 2, 3, 4, 5]. One popular neural network methods is the physics-informed neural networks (PINNs) [6], represent a significant advancement in the intersection of deep learning and scientific computing. PINNs incorporate physical constraints by embedding governing equations into the loss function. Alternatively, the deep Ritz method [7] and weak adversarial networks (WAN) [8] formulate the loss based on the weak form or variational form. The deep Ritz method solves PDEs by minimizing an energy function, and WAN converts the problem into an operator norm minimization problem. Despite the advancement of these methods, a major limitation is they are typically designed for a single PDE system instead of a series of PDEs, which means that a new model must be trained for each variation in parameters, initial conditions, or boundary conditions. In order to tackle this problem, operator learning frameworks like deep operator network (DeepONet) [9] and fourier neural operators (FNO) [10] were developed to learn the mappings between function spaces, enabling generalization across families of PDEs. DeepONet learns PDE solution operators by factorizing the operator into a branch network and

^{*}Corresponding Author: changma@ust.hk (Chang Ma), maxiang@ust.hk (Yang Xiang)

a trunk network, and FNO approximates the operators using global spectral convolutions in Fourier space. While these operator learning methods enable generalization across PDE families, they typically lack explicit stability guarantees, making their reliability highly sensitive to the propagation of input perturbations.

Stability is a cornerstone of analysis and design in traditional numerical methods, such as finite difference methods and finite element methods [11, 12]. By ensuring that errors do not amplify uncontrollably, it is a prerequisite for reliability and convergence, as rigorously formalized by tools like the Lax equivalence theorem and Von-Neumann analysis [13, 14]. Specifically, stability for tradition numerical methods requires that the discrete problem be well-posed, with the solution exhibiting a uniform bound, independent of the mesh resolution, on its sensitivity to perturbations in the data, i.e., source terms and initial/boundary conditions [15]. For ordinary differential equation, stability is often discussed when dealing with stiff equations, where an unstable numerical method can produce rapidly growing errors despite small step sizes [16, 17]. In the context of linear evolutionary PDEs, a numerical algorithm is considered stable if the total variation of the numerical solution at any fixed time remains bounded regardless of the temporal and spatial steps [16, 17]. In nonlinear cases, stability definitions must account for phenomena like shock formation and solution-dependent diffusion, often requiring problem-specific approaches to error control.

Unlike traditional numerical solvers, the stability properties of neural network-based PDE solvers remain insufficiently understood and lack a systematic theoretical framework despite the empirical success in many cases. Few works explicitly address stability and incorporate stability constraints into their training objectives or architectures, thereby leaving no guarantee that the learned solution remains stable under perturbations. Recently, uncertainty quantification [18] has emerged as a practical tool to assess the reliability of deep learning PDE solvers. These methods help identify regions where neural network predictions may be unstable or unreliable. Nevertheless, it serves as a diagnostic tool but does not enforce stability directly. Crucially, stability is a fundamental requirement for numerical solutions to PDEs in scientific and engineering contexts, since even minor perturbations in inputs, parameters, or source terms can lead to significant error propagation, non-physical oscillations, or even catastrophic divergence in the simulated system. Consequently, ensuring PDE stability is not merely a theoretical concern but a practical necessity for achieving reliable, safe, and credible computational outcomes.

The stability of neural networks has emerged as a critical safety concern in machine learning, particularly when deployed in high-stakes applications. Key studies focus on security-critical fields such as autonomous driving, facial recognition, and natural language processing [19, 20, 21]. The fragility of neural networks was starkly demonstrated by Goodfellow et al. [22], who showed that imperceptible perturbations – constructed by leveraging gradient information – could deceive classifiers into mislabeling images with high confidence, such as identifying a panda as a gibbon. Another example is that perturbing a "stop" sign could cause misclassification with potentially catastrophic consequences in autonomous driving. To mitigate these risks, adversarial training [23, 24] and other defense mechanisms [25, 26] have been proposed to improve the robustness of models. Adversarial learning provides a offensive yet rigorous framework by explicitly constructing worst-case perturbations that maximize model error. The gradient-based adversarial attack is one of the most widely studied methods for generating adversarial examples. These attacks exploit the gradients of loss function of machine learning models with respect to its input to craft perturbations that cause misclassification. The fast gradient sign method (FGSM) [22] is a single-step attack that perturbs inputs along the direction of the sign of the loss gradient, scaled by a small constant. Projected Gradient Descent (PGD)[23] obtains adversarial examples using a multistep variant of FGSM. PGD generalizes FGSM by applying iterative gradient updates with projection onto a constrained perturbation set, yielding much stronger and more reliable attack samples. Despite its higher computational cost, PGD exhibits improved robustness and

transferability across different models.

Despite their promise, challenges remain in addressing stability issues for neural network-based PDE solvers, as perturbations in physical system parameters can propagate errors in ways fundamentally different from those encountered in image classification tasks, thereby requiring tailored analytical frameworks. In image classification, for instance, small input perturbations—such as a slight rotation of a cat image—do not alter the underlying semantic label, which remains cat. In contrast, for PDE solvers, perturbations to input functions, including initial conditions, boundary data, or source terms, inherently modify the governing problem itself and thus change the true solution, making stability a problem of controlled solution sensitivity rather than label invariance.

In this work, we study the stability of neural operators for solving differential equations. Despite their strong empirical performance on normal data, we demonstrate that state-of-the-art neural operator architectures can exhibit severe instability under small but adversarial perturbations to input functions or physical parameters. To address this issue, we propose a stable training framework that formulates operator learning as a min–max optimization problem. It constrains the sensitivity of neural operators by training neural operators against worst-case input perturbations. Our approach combines adversarial training with operator learning, leading to stability guarantees that are analogous to those required of classical numerical PDE solvers. The resulting models maintain high accuracy on unperturbed inputs while exhibiting significantly improved robustness to worst-case perturbations. This work establishes a principled connection between adversarial robustness in machine learning and stability theory in numerical analysis, providing a foundation for reliable neural PDE solvers.

The remainder of the paper is organized as follows. We start with introducing our notation and preliminary results in section 2. In section 3, the StablePDENet framework and algorithm are proposed for enhancing the stability of the operator learning methods, which are based on the adversarial training. In section 4, the accuracy and efficiency of the proposed method are examined through several numerical experiments. Finally, this paper is concluded with general discussions in section 5.

2 Preliminaries

To conduct our research on the stability of neural PDE solvers, we first introduce the methods employed in this paper. The neural operator framework used here serves as an example and can be replaced with any operator learning framework.

2.1 Neural Operator Learning

An exemplary framework in operator learning is first presented for context. We use a self-supervised backend network, the Physics-Informed DeepONet (PIDeepONets) [27]. Following DeepONet, PIDeepONet also consists of two main components: a branch network and a trunk network. The branch network takes an input function (e.g. initial conditions) and encodes it into a feature representation, while the trunk network learns to evaluate the operator at specific points in the output space. Denote G_θ as the operator to be learned parametrized by θ , f as the input function, $G_\theta(f)$ as the output function, x as the points where the input function f is evaluated, y is the points where the output function $G_\theta(f)$ is evaluated. In the PIDeepONet, the branch net which takes in $\{f(x_1), f(x_2), \dots, f(x_m)\}$ as input, and outputs $[b_1, b_2, \dots, b_p]$ and the trunk net which takes in the points y in the domain of $G_\theta(f)$, and outputs $[t_1, t_2, \dots, t_p]$. The two

networks are merged by multiplication and may also be added with a bias:

$$G_\theta(f)(y) \approx \sum_{k=1}^p b_k t_k(+b_0) \quad (1)$$

The Physics-Informed DeepONet differs from DeepONet in that it is unsupervised and employs physics-informed loss. Given the equation, the domain, and the boundary condition, the losses contain the PDE loss and the boundary loss, where the PDE loss is the loss between the result after the input data is processed by the PDE and zero,

$$\mathcal{L}(\theta) = \mathcal{L}_{\text{physics}}(\theta) + \mathcal{L}_{\text{BC}}(\theta) + \mathcal{L}_{\text{IC}}(\theta), \quad (2)$$

where

$$\mathcal{L}_{\text{physics}}(\theta) = \mathcal{N}[G_\theta(f)](y), \quad (3)$$

\mathcal{N} means the physics laws the underlying functions obey. The physics laws may involve differentiation, and here automatic differentiation helps in computing. And \mathcal{L}_{BC} and \mathcal{L}_{IC} is the loss function on the boundary condition and initial condition, respectively. In order to clarify the notations, let us take the Poisson equation as an example. The 1D Poisson equation is written as

$$-u_{xx}(x) = f(x), \quad (4)$$

where $x \in [0, 1]$, $u(0) = u(1) = 0$. We wish to learn a map $G_\theta : f(x) \mapsto u(x)$, and the loss function is

$$\begin{aligned} \mathcal{L}(\theta) &= \mathcal{L}_{\text{physics}}(\theta) + \mathcal{L}_{\text{BC}}(\theta) \\ &= \frac{1}{Nm} \sum_{i=1}^N \sum_{j=1}^m \left\| \nabla^2 G_\theta(\mathbf{f}^{(i)})(y) \Big|_{y=x_j} - f^{(i)}(x_j) \right\|^2 + \frac{1}{N} \sum_{i=1}^N \left(\|G_\theta(\mathbf{f}^{(i)})(0)\|^2 + \|G_\theta(\mathbf{f}^{(i)})(1)\|^2 \right) \end{aligned} \quad (5)$$

where $\mathbf{f}^{(i)} = [f^{(i)}(x_1), f^{(i)}(x_2), \dots, f^{(i)}(x_m)]$, $\|\cdot\|$ represent 2-norm of the vector.

2.2 Adversarial Training

Adversarial training was formalized by Madry et al. [23] as a min-max optimization problem:

$$\min_{\theta} \mathbb{E}_{(x,y) \sim \mathcal{D}} \left[\max_{\|\delta\|_\infty \leq \varepsilon} \mathcal{L}(f_\theta(x + \delta), y) \right],$$

where f_θ is the neural network, δ is the adversarial perturbation bounded by ε , \mathcal{L} is the loss function, and y is the label. This formulation interprets adversarial training as a two-player game: on one hand, the adversary maximizes the loss by finding the worst-case perturbation; on the other hand, the model minimizes the expected adversarial loss. Generally, the PGD training model is trained on adversarial examples generated by (6), improving robustness against strong attacks. With the initialization $x^0 = x$ where x is the input, the perturbed data in the t -th step x^t can be expressed as follows:

$$x^t = \Pi_{x+S}(x^{t-1} + \alpha \cdot \text{sign}(\nabla_x L(f_\theta(x^{t-1}), y))) \quad (6)$$

where L is the loss, x is the input, y is the label, f is the neural network, θ is the parameters of the model, Π_{x+S} denotes projecting perturbations into the set S , S is the set constrained by l_∞ or l_2 ball (i.e. $S = \{x, \|x\|_\infty < \varepsilon\}$ or $S = \{x, \|x\|_2 < \varepsilon\}$), ε is the allowed perturbation size, and α is the step size. We denote PGD bounded by l_∞ as the PGD-inf attack, and PGD bounded by l_2 as the PGD- l_2 attack. The PGD-inf creates sparse but perceptible noise, typically characterized by small localized distortions, and the PGD- l_2 produces perturbations more evenly across input features, resulting in subtler but broader modifications.

3 StablePDENet

Conventional neural operator training relies on minimizing empirical risk using standard optimization methods, which do not enforce stability constraints and can lead to unstable predictions when faced with input perturbations, noise, uncertainties, or out-of-distribution samples. In order to address this, we propose a stability-enhancing framework for neural network-based PDE solvers, named StablePDENet. It leverages adversarial training to implicitly enforce stability constraints. We first introduce the concept of the stability of neural operators for solving PDEs and show that our method implicitly controls the boundedness of the Fréchet derivative of operator. Important implementation details of the adversarial training algorithm are also provided. Figure 1 illustrates the idea of the StablePDENet with a sketch.

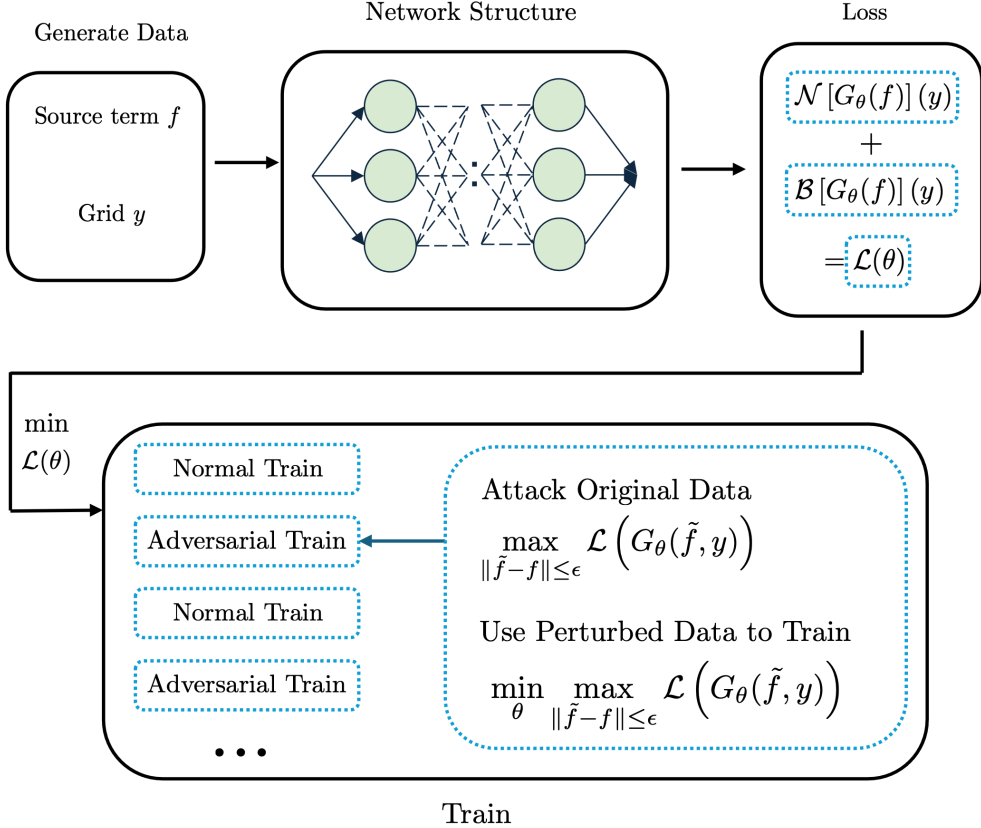


Figure 1: The architecture of StablePDENet.

3.1 StablePDENet based on Adversarial Training

We consider representing the solutions to partial differential equations by the neural networks with parameters θ . The neural PDE solver is defined as an operator $G_\theta : \mathcal{F} \rightarrow \mathcal{U}$ that maps given conditions $f \in \mathcal{F}$ to the neural network solution u_θ , where $(\mathcal{F}, \|\cdot\|_{\mathcal{F}})$ represents the input function space including admissible initial conditions, boundary conditions or coefficients or source terms, and $(\mathcal{U}, \|\cdot\|_{\mathcal{U}})$ is the solution space. Furthermore, the neural operator G_θ is a finite composition of bounded linear operators and pointwise nonlinearities $\sigma \in C^1(\mathbb{R}) \cap W^{1,\infty}(\mathbb{R})$ (Tanh, Sigmoid, etc.). Consequently, G_θ and its Fréchet derivative DG_θ exists. Consistent with the classical concepts of stability for numerical schemes, we define the following stability criterion for neural network approximations.

Definition 3.1 (Stability in Neural PDE Solvers). *The Neural PDE solver is said to be **stable** if there exist constants $C > 0$, $\delta_0 > 0$ such that for all perturbations $\delta \in \mathcal{F}$ with $\|\delta\|_{\mathcal{F}} \leq \delta_0$, and*

for all input conditions $f \in \mathcal{F}$, the following inequality holds:

$$\|G_\theta(f + \delta) - G_\theta(f)\|_{\mathcal{U}} \leq C\|\delta\|_{\mathcal{F}},$$

where the stability constant C is parameter-independent, which can be achieved by restricting parameters to a bounded set or applying regularization techniques during training.

To satisfy the stability in Definition 3.1 implicitly, we employ the adversarial training method in operator learning for solving PDEs. The core of our approach lies in formulating the operator learning problem as a min-max optimization. Building on the self-supervised learning framework of PIDeepONet without input-output pairs as labels, the adversarial training objective is formally expressed as follows,

$$\min_{\theta} \max_{\|\tilde{f} - f\| \leq \varepsilon} \mathcal{L}(G_\theta(\tilde{f}, y)), \quad (7)$$

where \mathcal{L} is the physics-informed loss function, \tilde{f} is the input perturbation, y is the evaluation points, δ is the perturbation of input data, ε defines the perturbation radius. In addition, (7) is equivalent to minimizing the worst-case loss induced by admissible perturbations of the input function within an ε -ball in the input space \mathcal{F} ,

$$\sup_{\|\delta f\|_{\mathcal{F}} \leq \varepsilon} \mathcal{L}(G_\theta(f + \delta f)) \quad (8)$$

This formulation measures the maximum discrepancy between the neural operator prediction and the reference solution, thereby capturing a notion of worst-case robustness.

Through adversarial training, the operator becomes robust to input noise and distribution shifts by exposure to challenging perturbations during the training. To reveal the connection between adversarial robustness and operator stability rigorously, we perform a first-order Taylor expansion of the loss with respect to the input perturbation. For sufficiently small ε , this yields

$$\sup_{\|\delta f\|_{\mathcal{F}} \leq \varepsilon} \mathcal{L}(G_\theta(f + \delta f)) = \mathcal{L}(G_\theta(f)) + \varepsilon \|\nabla_f \mathcal{L}(G_\theta(f))\|_{\mathcal{F}^*} + o(\varepsilon) \quad (9)$$

where $\nabla_f \mathcal{L}(G_\theta(f)) = [DG_\theta(f)]^* \nabla \mathcal{L}(G_\theta(f))$, $DG_\theta(f)$ denotes the Fréchet derivative/Jacobian of the neural operator at f , \mathcal{F}^* denotes the dual space of the input function space \mathcal{F} , $DG_\theta(f)^*$ is the adjoint of the Fréchet derivative of the neural operator. This expansion shows that the dominant contribution of the adversarial perturbation is that the magnitude of operator norm of the derivative DG_θ is controlled. Consequently, minimizing the perturbed loss in (8) implicitly enforces a uniform bound on $\|DG_\theta\|$. This guarantees that small perturbations in the input lead to proportionally bounded variations in the output, thus promoting stability of the neural operator in the sense of Definition 3.1.

Figure 1 presents the comprehensive framework of our stability-enhanced neural operator. We first generate data i.e., input function f and grid data. Then, the branch network processes input functions f and produces feature embedding $b(f)$, and the trunk network handles coordinate inputs y and generates $t(y)$. The network outputs the dot product of $b(f)$ and $t(y)$, and also adds a bias b_0 in the last stage. The training process employs a composite loss function following (2) and (3) without solution data label. The training process of the StablePDENet is composed of two processes, attack process and defense process. The maximization process is the attack process, and the minimization process is the defense process. Specifically, we use normal training in the initial phase. This process establishes a baseline solution manifold and provides reference gradients for the defense phase. In the subsequent phases, we use adversarial training and normal training alternately. Finally, we train iteratively using normal training and adversarial training using physics-informed loss, where we simultaneously:

- **Attack:** Generate challenging perturbations that expose model weaknesses (maximization)
- **Defense:** Improve model robustness against these perturbations (minimization)

3.2 Training algorithm for Attack and Defense

For the attack process, the resulting algorithm, termed as Attack in adversarial training, is Algorithm 1. It implements the PGD attack described, which computes adversarial directions through gradient ascent while projecting perturbations onto the feasible set $\|\tilde{f} - f\| \leq \varepsilon$ at each iteration. Note that we employ the physics-informed loss as a surrogate for the true solution error, avoiding expensive recomputation of numerical solutions for each perturbation during training. The complete adversarial training algorithm implements an online learning paradigm.

Algorithm 1 Attack in adversarial training $(\max_{\|\tilde{f}-f\| \leq \varepsilon} \mathcal{L}(G_\theta(\tilde{f}, y)))$

Require: Input function f , coordinates y , pretrained model G_θ ;
Require: Attack parameters: step size α , perturbation bound ε , iterations n_{iter} ;
 Initialize: $\tilde{f} \leftarrow f + \delta$, $\delta \sim \mathcal{U}(-\varepsilon, \varepsilon)$ {Random warm-start}
for $i = 1$ to n_{iter} **do**
 Compute $\mathcal{L}(\theta) = \mathcal{L}_{\text{physics}}(\theta) + \mathcal{L}_{\text{BC}}(\theta) + \mathcal{L}_{\text{IC}}(\theta)$ {Physics-informed loss}
 Compute gradient: $g \leftarrow \nabla_{\tilde{f}} \mathcal{L}$
 Update: $\tilde{f} \leftarrow \tilde{f} + \alpha \cdot \text{sign}(g)$ {Sign gradient ascent}
 Project: $\tilde{f} \leftarrow \text{Clip}(\tilde{f}, f - \varepsilon, f + \varepsilon)$ {Maintain ℓ_∞ bound}
end for
return (\tilde{f}, y)

Algorithm 2 Adversarial Training Algorithm $(\min_\theta \max_{\|\tilde{f}-f\| \leq \varepsilon} \mathcal{L}(G_\theta(\tilde{f}, y)))$

Require: Initial parameters θ_0 , training steps N , learning rate η ;
Require: Attack step size α , perturbation bound ε , attack iterations k
for training step $j = 1$ to N **do**
 Generate new input function $f_t \sim \mathcal{P}$ {Sample from problem distribution}
 while $i < k$ **and** $M \mid j$ **do**
 Generate adversarial example (\tilde{f}, y) using **Algorithm 1** with:
 - Current model G_{θ_t}
 - Input pair (f_t, y_t)
 - Attack step size α , perturbation bound ε , attack iterations k
 end while
 Compute training loss:
 $\mathcal{L}(\theta) = \mathcal{L}_{\text{physics}}(\theta) + \mathcal{L}_{\text{BC}}(\theta) + \mathcal{L}_{\text{IC}}(\theta)$
 Update model parameters:
 $\theta_{t+1} \leftarrow \theta_t - \eta \nabla_\theta \mathcal{L}_t$
end for
return G_θ

Overall, the implement of the StablePDENet is summarized in Algorithm 2. Within the core architecture of training algorithm, every optimization iteration dynamically synthesizes novel input functions from a predefined function space, fundamentally circumventing the risk of overfitting to any static dataset. This continuous regeneration strategy ensures the model encounters an ever-evolving distribution of input patterns throughout the training trajectory, systematically enhancing generalization capabilities to unseen physical scenarios. Crucially, our physics-informed training loss is intrinsically embedded throughout the adversarial learning pipeline. This framework provides a principled approach to developing PDE solution operators that are both accurate

and robust to input perturbations.

4 Numerical Experiments

In this section, we conduct a set of numerical experiments to show the practical performance of the StablePDENet in solving parametric ODEs or PDEs with perturbed inputs. Table 1 shows problem settings for assessing the performance of our method across various types of parametric differential equations with various types of perturbed terms.

Governing law	Equation form	Perturbed term
Linear ODE	$\frac{du}{dt} = f(x)$	Forcing terms
Possion Eq.	$-\frac{\partial^2 u(x)}{\partial x^2} = f(x)$	Source terms
	$-\left(\frac{\partial^2 u}{\partial x^2} + \frac{\partial^2 u}{\partial y^2}\right) = f(x, y)$	Source terms
Elliptic Eq.	$-\Delta u + 2u = f$	Source terms
Heat Eq.	$\frac{\partial u(x,t)}{\partial t} - \alpha \frac{\partial^2 u(x,t)}{\partial x^2} = 0$	Initial conditions
	$\frac{\partial u(x,t)}{\partial t} - \alpha \frac{\partial^2 u(x,t)}{\partial x^2} = f(x)$	Source terms
Diffusion reaction	$\frac{\partial u(x,t)}{\partial t} - D \frac{\partial u(x,t)}{\partial x^2} - ku^2(x,t) - f(x,t) = 0$	Source terms Variable coefficients
Stokes Eq.	$\mu \Delta u - \nabla p = 0,$ $\nabla u = 0$	Boundary conditions

Table 1: Problem settings for assessing the performance of the StablePDENet across various types of parametric differential equations with various types of perturbed terms.

Generally, the networks for the branch net and trunk net are both 3-layer fully connected neural networks with 128 neurons per layer, and both employ tanh activation functions and are initialized using the Glorot normal distribution. All models are trained by Adam with 50000 steps. In each step, the batch size is 100. Moreover, input functions f_i are sampled from a function space \mathcal{U} capturing the expected parameter space of the PDE problem. The functions f_i are evaluated on the sensors x_1, x_2, \dots, x_m . The grid data y is the grid at which the output functions are evaluated, which are not necessarily equal to $\{x_i\}_{i=1}^m$. In addition, for the experiments involving two-dimensional spatial domains 4.2.2 and 4.6, the network outputs are transformed to ensure that the initial conditions or boundary conditions are satisfied for facilitate training.

To assess the performance and robustness of the proposed framework, we establish two test datasets to evaluate different aspects of model performance:

- Base Performance Dataset ($\{f(x_i)\}_{i=1}^m, y, u_{\text{true}}(y)$): Pairs of unperturbed source terms f and their corresponding numerical solutions u_{true} generated using validated PDE solvers. This dataset evaluates the model's inherent accuracy on clean inputs.
- Robustness Evaluation Dataset ($\{\tilde{f}(x_i)\}_{i=1}^m, y, \tilde{u}_{\text{true}}(y)$): Pairs of adversarially perturbed source terms \tilde{f} and their recomputed numerical solutions \tilde{u}_{true} . This dataset specifically assesses stability under perturbations which are generated using the gradient-based attack method.

The generation of these datasets involves three computational stages: First, we generate the original source terms f and compute their numerical solutions u_{true} using validated PDE solvers.

Second, we apply adversarial perturbations (10) to each f to construct corrupted inputs \tilde{f} .

$$\max_{\|\tilde{f}-f\| \leq \varepsilon} \mathcal{L}\left(G_\theta(\tilde{f}, y), u_{\text{true}}\right) \quad (10)$$

Algorithm A1 in the Appendix provides a formal pseudocode for generating \tilde{f} . Third, we recompute the numerical solutions \tilde{u}_{true} for these perturbed sources to establish reference solutions for the robustness assessment. In addition, each dataset containing 2,000 input-solution pairs for comprehensive error analysis. We compute the relative L^2 error $\|G_\theta(f) - u\|_2 / \|u\|_2$ on both inputs of both training methods. Through this rigorous methodology, we establish performance baselines that account for both error in normal cases and stability under input perturbations.

4.1 Parametric Ordinary Differential Equation with Force Perturbed

To begin with, we first illustrate an elementary example involving the antiderivative operator. The underlying governing law corresponds to an initial value problem described by the following ordinary differential equation with zero initial condition

$$\begin{cases} \frac{du(x)}{dx} = f(x), & x \in [0, 1] \\ u(0) = 0 \end{cases} \quad (11)$$

The problem aims to learn the operator that maps the function $f(x)$ to $u(x)$, which is written as

$$G : f(x) \longrightarrow u(x) = u(0) + \int_0^x f(t)dt, \quad x \in [0, 1]. \quad (12)$$

The model is trained on random realizations of $f(x)$, and tested on new unseen realizations that are not used during the model training. We train the two models with the loss

$$\begin{aligned} \mathcal{L}(\theta) &= \mathcal{L}_{\text{physics}}(\theta) + \mathcal{L}_{\text{IC}}(\theta) \\ &= \frac{1}{Nm} \sum_{i=1}^N \sum_{j=1}^m \left\| \frac{dG_\theta(\mathbf{f}^{(i)})(y)}{dy} \Big|_{y=x_j} - f^{(i)}(x_j) \right\|^2 + \frac{1}{N} \sum_{i=1}^N \left\| G_\theta(\mathbf{f}^{(i)})(0) \right\|^2, \end{aligned} \quad (13)$$

where $\mathbf{f}^{(i)} = [f^{(i)}(x_1), f^{(i)}(x_2), \dots, f^{(i)}(x_m)]$ ($m = 50$) represents the input function. We optimize using the Adam algorithm for 40000 iterations.

To generate data for training, we sample random realizations of $f(x)$ from a Gaussian random field with a radial basis kernel and a length scale of $l = 0.2$, and the functions are evaluated on uniformly distributed 50 sensors on $[0, 1]$. The output solutions $u(y)$ are evaluated by the Hammersley distributed locations in $[0, 1]$ with 20 points, concatenated with the initial point. The batch size is 100, and for every step, we generate a new batch of realizations of $f(x)$ for training. For measuring the performance, we predict the network output and discretize the u_{true} both on a uniformly distributed 50 points on $[0, 1]$. In order to study the accuracy for the model after training, we compute the corresponding numerical solutions $u_{\text{true}}(x)$ to 2000 ODEs using explicit Runge-Kutta method of order 5(4).

The numerical results for three representative samples are presented in Figure 2. The left column illustrates the original source term $f(x)$ alongside its adversarially perturbed counterpart $\tilde{f}(x)$ generated by our proposed attack method. The middle column compares the predicted solutions of PIDeepONet and the StablePDENet against the exact solutions for the unperturbed source terms. Both approaches demonstrate comparable accuracy, closely aligning with the ground truth. In contrast, the right column assesses the models performance under adversarial

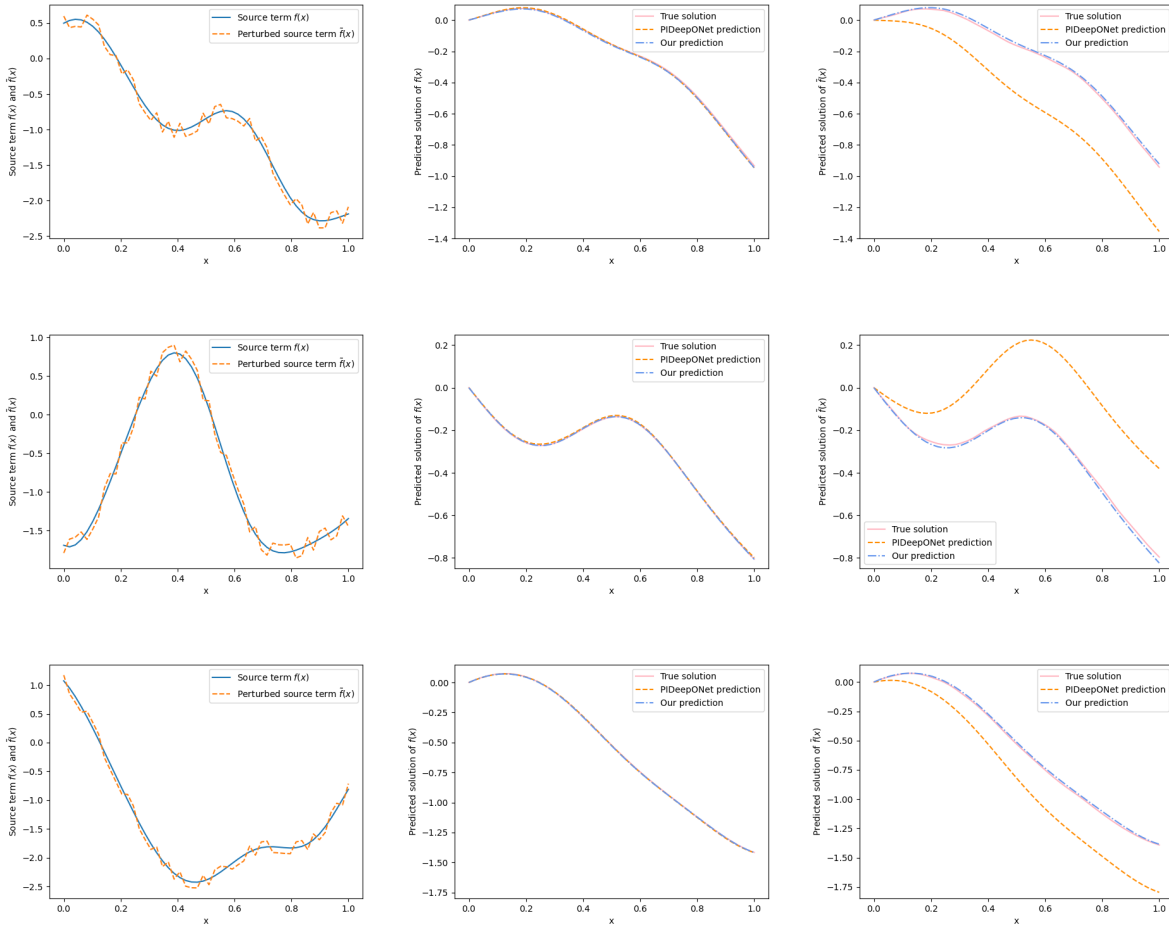


Figure 2: Solving a 1D parametric ODE: Left: The original source term and the perturbed source term; Middle: Solutions w.r.t. the original source term; Right: Solutions w.r.t. the perturbed source term.

perturbation. The StablePDENet maintains high fidelity to the exact solutions, but the prediction results of PIDeepONet exhibit significant deviations, completely losing robustness. This stark difference underscores the superior stability of our approach against adversarial distortions. These results suggest that while existing methods perform well under ideal conditions, the additional robustness considerations in our framework provide meaningful advantages when dealing with input uncertainties or perturbations, a common requirement in real-world applications. The improved stability comes without sacrificing accuracy on normal inputs, representing a valuable step toward more reliable operator learning.

Table 2 shows the relative L^2 error of the PIDeepONet prediction and our prediction compared to the true numerical solution. We can see that while both our method and PIDeepONet achieve high accuracy on unperturbed data, our approach demonstrates marginally superior performance, likely attributable to the adversarial training component in our optimization framework. This training paradigm appears to enhance generalizability even for normal inputs by promoting smoother loss landscapes. However, the critical distinction emerges under adversarial perturbation: PIDeepONet suffers catastrophic failure, whereas our method maintains robust performance. This stark contrast underscores how adversarial training not only preserves accuracy on original data but is essential for maintaining stability when inputs are perturbed.

Relative L^2 error w.r.t. true solution		
Network	Data	Relative L^2 error
PIDeepONet	Original data	0.019
StablePDENet	Original data	0.012
PIDeepONet	Attacked data	0.740
StablePDENet	Attacked data	0.058

Table 2: Parametric Ordinary Differential Equation

4.2 Poisson Equation

4.2.1 1D Poisson Equation with Source Perturbed

The next equation that we try to solve is the one-dimensional Poisson equation.

$$\begin{cases} -\frac{\partial^2 u(x)}{\partial x^2} = f(x), & x \in [0, 1] \\ u(0) = 0 \\ u(1) = 0 \end{cases} \quad (14)$$

The aim is to learn the operator that maps the source function $f(x)$ to $u(x)$,

$$G : f(x) \longrightarrow u(x), \quad x \in [0, 1]. \quad (15)$$

The loss we use is (5).

We generate the source functions f from a function space consisting of polynomials of degree 3. These functions are evaluated on sensors 100 points uniformly distributed on $[0, 1]$. The output functions are discretized on 100 points on $[0, 1]$ with a Hammersley distribution, along with two points on the boundary. We use 2000 examples to test the performance of the two models, where the test functions are evaluated on $[0, 1]$ with 100 points uniformly distributed, and compute the numerical solutions corresponding to f and \tilde{f} using the finite difference method.

Figure 3 shows the results of three representative samples. Similarly, the left column shows the original source terms $f(x)$ and their adversarially perturbed counterparts $\tilde{f}(x)$ generated by our proposed method. The middle column demonstrates that both PIDeepONet and our method achieve excellent agreement with the ground truth solutions for unperturbed inputs. This confirms that conventional physics-informed operator learning methods can provide highly accurate solutions for standard input conditions. However, the right column reveals important differences in model robustness when subjected to adversarial perturbations. Our method maintains high accuracy even under input perturbations. The error statistics are shown Table 3 below, which also verify our claim.

Relative L^2 error w.r.t. true solution		
Network	Data	Relative L^2 error
PIDeepONet	Original data	0.013
StablePDENet	Original data	0.005
PIDeepONet	Attacked data	10.541
StablePDENet	Attacked data	0.012

Table 3: 1D Poisson Equation

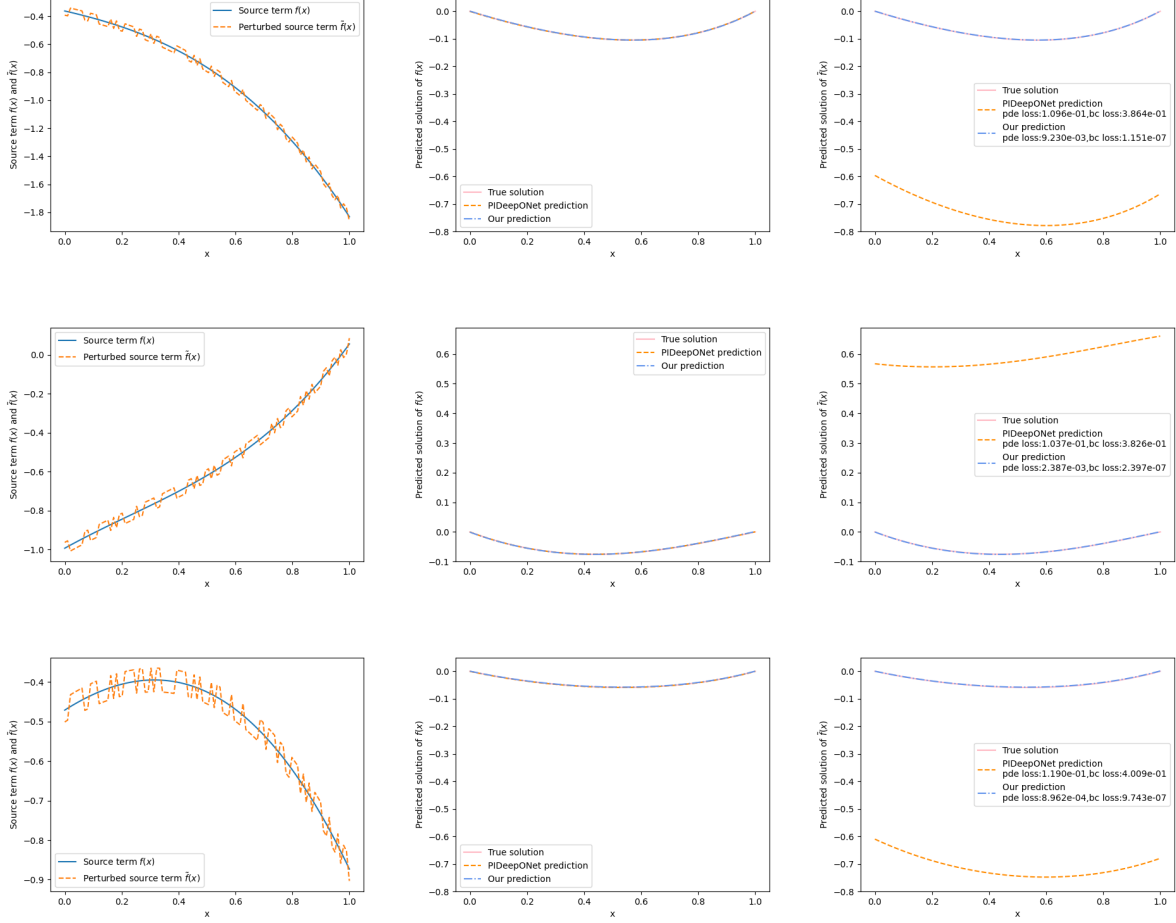


Figure 3: Solving a 1D Poisson equation: Left: The original source term and the perturbed source term; Middle: Solutions w.r.t. the original source term; Right: Solutions w.r.t. the perturbed source term.

4.2.2 2D Possion Equation with Source Perturbed

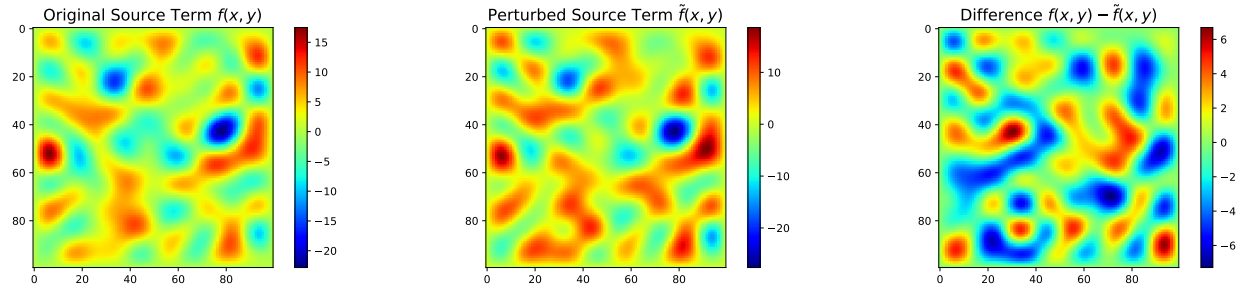
Additionally, we also consider the two-demensional Possion equation,

$$\begin{cases} -\left(\frac{\partial^2 u}{\partial x^2} + \frac{\partial^2 u}{\partial y^2}\right) = f(x, y), & (x, y) \in (0, 1)^2 \\ u(x, 0) = u(x, 1) = 0, x \in (0, 1) \\ u(0, y) = u(1, y) = 0, y \in (0, 1) \end{cases} \quad (16)$$

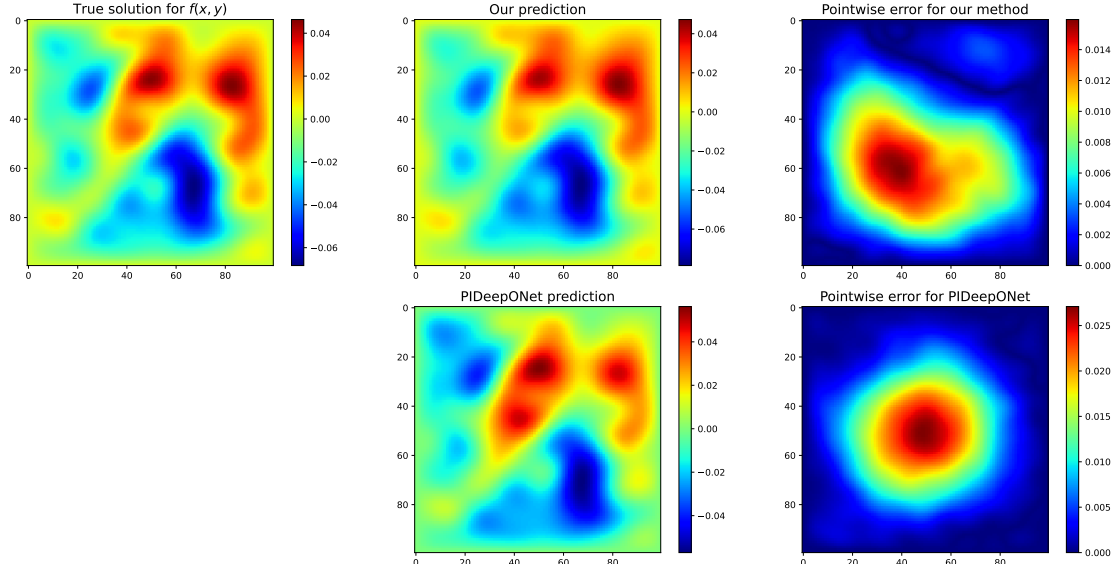
As in the previous example, we also learn an operator mapping from the source term $f(x, y)$ to the solution $u(x, y)$. The source term $f(x, y)$ is assumed to possess the following bi-trigonometric form:

$$f(x, y) = \sum_{r=1}^R \sum_{s=1}^S c_{rs} \sin(r\pi x) \sin(s\pi y) \quad (17)$$

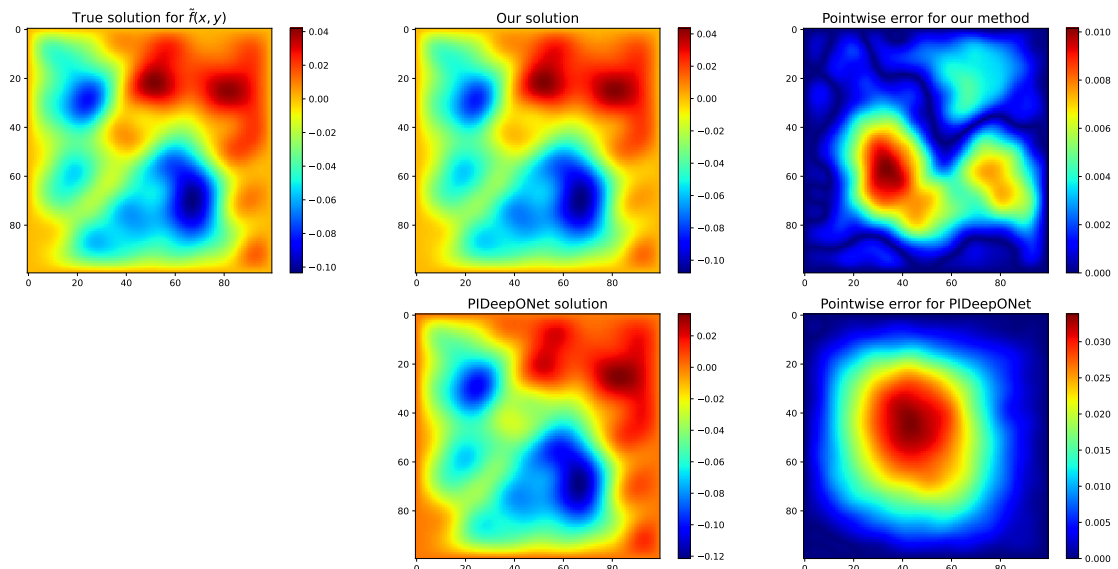
whereby an analytical solution exists for validation. We sample 1080 sets od the coefficients c_{rs} from $\mathcal{N}(0, 1)$ assuming $R = S = 10$. We use batch size $M = 36$ and evaluation points $N = 10000$ for training.



(a)



(b)



(c)

Figure 4: Solving 2D Possion equation: one example. (a) The original source term and the perturbed source term; (b) Solutions w.r.t. the original source term; (c) Solutions w.r.t. the perturbed source term.

Figure 4 shows the test results of a representative sample. The top row shows the original source term $f(x, y)$ and their adversarially perturbed counterparts $\tilde{f}(x, y)$. Figure 4(b) demonstrates that the StablePDENet and PIDeepONet can match the true solution for unperturbed inputs. However, Figure 4(c) reveals our method significantly outperforms PIDeepONet in model robustness when subjected to adversarial perturbations. The error statistics are shown below Table 4, the relative errors of our method and PIDeepONet for unperturbed inputs should converge to around 10%, but the relative errors of PIDeepONet for perturbations reach 50%, which also verify our claim.

Relative L^2 error w.r.t. true solution		
Network	Data	Relative L^2 error
PIDeepONet	Original data	0.113
StablePDENet	Original data	0.105
PIDeepONet	Attacked data	0.532
StablePDENet	Attacked data	0.097

Table 4: 2D Poisson Equation

4.3 Elliptic Equation with Neumann Boundary

We then test our method on a Helmholtz equation with Neumann boundary conditions.

$$\begin{cases} -\Delta u + 2u = f & \text{in } \Omega \\ \frac{\partial u}{\partial n} = 0 & \text{on } \partial\Omega \end{cases} \quad (18)$$

The domain $\Omega = [0, 1]$.

Similar to the case in Section 4.1, we generate the source functions from a Gaussian random field with a radial basis kernel and a length scale of $l = 0.2$, and the functions are evaluated on uniformly distributed 100 sensors on $[0, 1]$. The output $u(y)$ is evaluated by the Hammersley distributed locations in $[0, 1]$ with 100 points, concatenated with the initial point. The batch size is 50, and for every step, we generate a new batch of realizations of $f(x)$ for training.

Figure 5 shows the results of three examples. Same as before, the left panel illustrates the original source term $f(x)$ along with its adversarially perturbed counterpart $\tilde{f}(x)$ generated by our proposed attack method. The middle panels compare the predicted solutions of PIDeepONet and the StablePDENet against the exact solutions for the unperturbed source terms, while the right panels evaluate model performance under adversarial perturbation. Table 5 shows the relative l^2 errors of the predictions of the methods compared with the true solutions. We can see that for the Neumann boundary condition problems, our method still shows superiority compared to the PIDeepONet.

Relative L^2 error w.r.t. true solution		
Network	Data	Relative L^2 error
PIDeepONet	Original data	0.019
StablePDENet	Original data	0.022
PIDeepONet	Attacked data	0.720
StablePDENet	Attacked data	0.029

Table 5: Elliptic PDE with Neumann Boundary

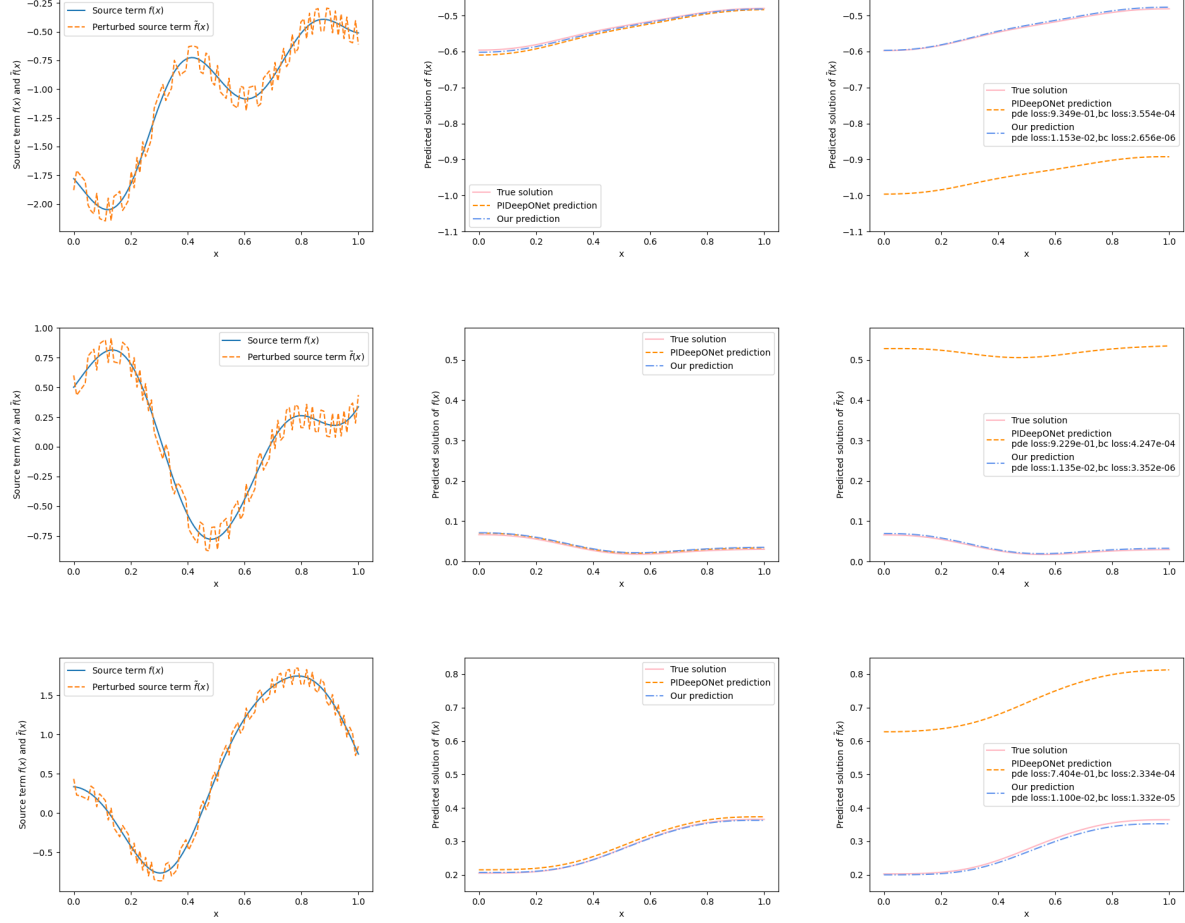


Figure 5: Solving Elliptic equation with Neumann boundary: Left: The original source term and the perturbed source term; Middle: Solutions w.r.t. the original source term; Right: Solutions w.r.t. the perturbed source term.

4.4 Heat Equation

4.4.1 Heat Equation with Initial Condition Perturbed

We consider the heat equation in $(x, t) \in \Omega$, with Dirichlet zero boundary condition and the initial condition is the input function $f(x)$, where $\Omega = [0, 1]$, $\alpha = 0.01$, and show the result in the time domain $[0, 1]$.

$$\begin{cases} \frac{\partial u(x,t)}{\partial t} - \alpha \frac{\partial^2 u(x,t)}{\partial x^2} = 0 & \text{in } \Omega \\ u(x, 0) = f(x) \\ u(x, t) = 0 & \text{on } \partial\Omega \end{cases} \quad (19)$$

The goal is to learn the operator:

$$G : f(x) \longrightarrow u(x, t = 1), \quad x \in [0, 1].$$

The loss we use is

$$\begin{aligned}
\mathcal{L}(\theta) &= \mathcal{L}_{\text{physics}}(\theta) + \mathcal{L}_{\text{BC}}(\theta) + \mathcal{L}_{\text{IC}}(\theta) \\
&= \frac{1}{Nm} \sum_{i=1}^N \sum_{p=1}^m \sum_{q=1}^n \left\| \partial_t G_\theta \left(\mathbf{f}^{(i)} \right) (x, t) \Big|_{x=x_q, t=t_p} - \alpha \partial_{x^2}^2 G_\theta \left(\mathbf{f}^{(i)} \right) (x, t) \Big|_{x=x_q, t=t_p} \right\|^2 + \\
&\quad \frac{1}{N} \sum_{p=1}^m \left\| G_\theta \left(\mathbf{f}^{(i)} \right) (0, t_p) \right\|^2 + \frac{1}{N} \sum_{p=1}^m \left\| G_\theta \left(\mathbf{f}^{(i)} \right) (1, t_p) \right\|^2 + \frac{1}{N} \sum_{q=1}^n \left\| G_\theta \left(\mathbf{f}^{(i)} \right) (x_q, 0) - (\mathbf{f}^{(i)} (x_q)) \right\|^2
\end{aligned} \tag{20}$$

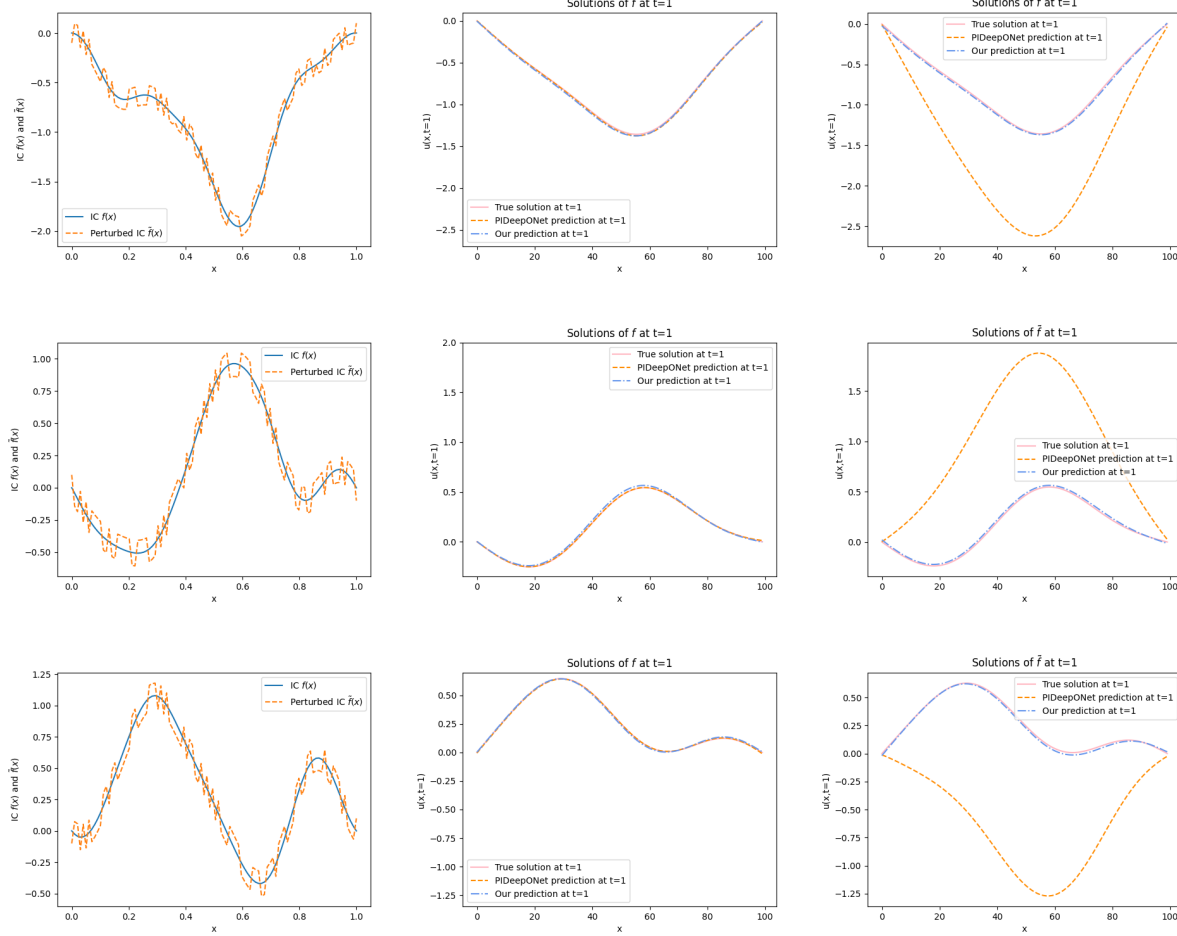


Figure 6: Solving Heat Equation with Initial Condition Perturbed: Left: The original source term and the perturbed source term; Middle: Solutions w.r.t. the original source term; Right: Solutions w.r.t. the perturbed source term.

We generate the source functions f from a Gaussian random field with a radial basis kernel and a length scale of $l = 1$. These functions are evaluated on sensors 100 points uniformly distributed on $[0, 1]$. The output functions are discretized on 200 points on $[0, 1] \times [0, 1]$ with a Hammersley distribution, along with 20 points on the initial time $t = 0$ and 40 points on the boundaries. We use 2000 examples to test the performance of the two models, where the test solution functions are evaluated on $[0, 1] \times [0, 1]$ with 100×100 points uniformly distributed. We compute the numerical solutions corresponding to f and \tilde{f} using the finite difference method.

Figure 6 shows both for the original source term and for their adversarially perturbed coun-

terparts, our method achieve higher accuracy than PIDeepONet for unperturbed inputs. The evaluation statistics are shown on Table 6. The relative error of PIDeepONet after perturbation reaches as high as 59%, while our model remain very stable.

Relative L^2 error w.r.t. true solution		
Network	Data	Relative L^2 error
PIDeepONet	Original data	0.019
StablePDENet	Original data	0.034
PIDeepONet	Attacked data	0.591
StablePDENet	Attacked data	0.036

Table 6: Heat Equation with Initial Condition Perturbed

4.4.2 Inhomogeneous Heat Equation with Source Perturbed

We consider the inhomogeneous heat equation in $(x, t) \in \Omega$, with homogenous Dirichlet boundary condition and zero initial condition, where $\Omega = [0, 1]$, and show the result in the time domain $[0, 1]$.

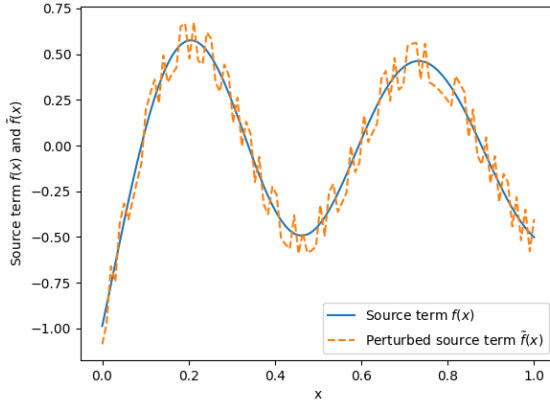
$$\begin{cases} \frac{\partial u(x,t)}{\partial t} - \alpha \frac{\partial^2 u(x,t)}{\partial x^2} = f(x) & \text{in } \Omega \\ u(x, 0) = 0 \\ u(x, t) = 0 & \text{on } \partial\Omega \end{cases} \quad (21)$$

We generate the source functions $f(x)$ from a Gaussian random field with a radial basis kernel and a length scale of $l = 0.2$. The other parameter settings for this experiment are the same as those in the previous experiment.

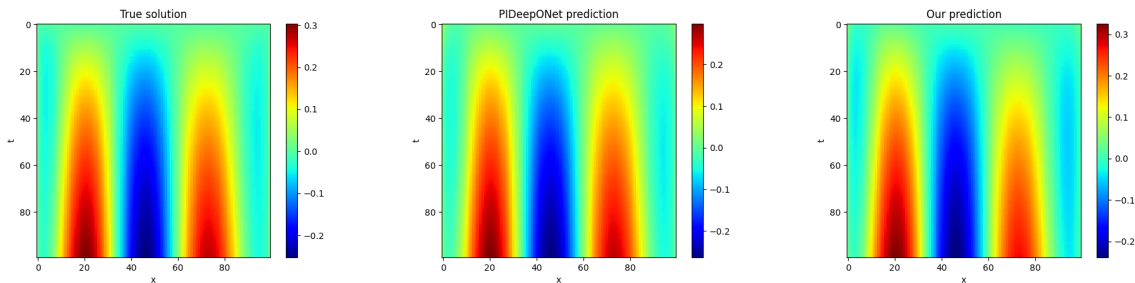
We plot the results of one example in Figure 7. The first row shows the original source term and the perturbed source term. The second row compares the corresponding solutions for the unperturbed source function $f(x)$, where the three panels are arranged as follows: the numerical reference solution, the PIDeepONet prediction, and the StablePDENet prediction. Similarly, the third row represents the solutions for the perturbed source function $\tilde{f}(x)$, following the same left-to-right order. We can see that for the unperturbed input, the predictions of both models align well with the numerical solution. However, the PIDeepONet loses its advantage once perturbed; meanwhile, our model maintains its performance. The relative errors are shown below. Our model is stable under perturbation, while the error of PIDeepONet has diverged.

Relative L^2 error w.r.t. true solution		
Network	Data	Relative L^2 error
PIDeepONet	Original data	0.024
StablePDENet	Original data	0.042
PIDeepONet	Attacked data	0.728
StablePDENet	Attacked data	0.047

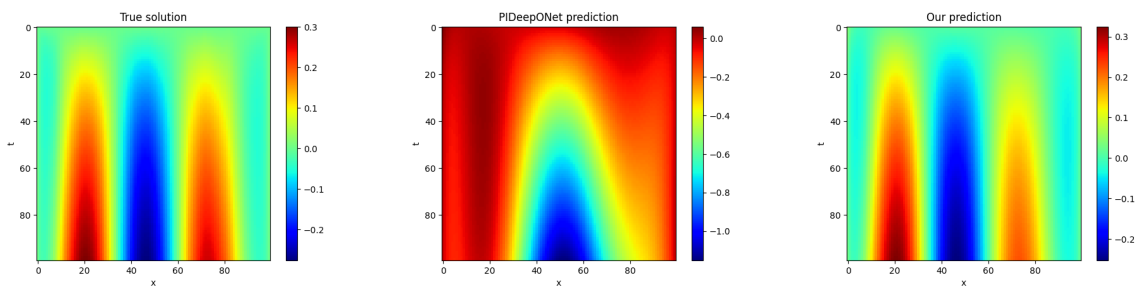
Table 7: Inhomogeneous Heat Equation



(a)



(b)



(c)

Figure 7: Solving inhomogeneous heat equation: one example. (a) The original source term and the perturbed source term; (b) Solutions w.r.t. the original source term; (c) Solutions w.r.t. the perturbed source term.

4.5 Diffusion Reaction Equation

4.5.1 Diffusion Reaction Equation with Source Perturbed

The diffusion-reaction equation is a partial differential equation that models the behavior of substances undergoing diffusion and chemical reactions simultaneously. It describes how the concentration of a substance changes over time and space due to two main processes: the spreading of particles and the transformation of particles through chemical reactions.

$$\frac{\partial u(x, t)}{\partial t} - D \frac{\partial^2 u(x, t)}{\partial x^2} - k u^2(x, t) - f(x, t) = 0, \quad x \in [0, 1], t \in [0, 1]. \quad (22)$$

where $D = k = 0.01$. The boundary condition is the homogeneous Dirichlet boundary condition, and the initial condition is also the zero condition.

We learn an operator mapping from the source term $f(x, t)$ to the solution $u(x, t)$. The corresponding physics loss is

$$\mathcal{L}_{\text{physics}}(\theta) = \frac{\partial G_\theta(f)(x, t)}{\partial t} - D \frac{\partial^2 G_\theta(f)(x, t)}{\partial x^2} - k [G_\theta(f)(x, t)]^2 - f(x, t) \quad (23)$$

The function $f(x, t)$ is the input function and depends only on the variable x , i.e., $f(x, t) = f(x)$. In the experiments, we generate the function f from a Gaussian random field with radial basis function kernel with length $l = 0.2$. We sample 200 points in the domain, 40 points for the boundary, 20 points for the initial condition. We test 2000 input examples for assessing the performance of the PIDDeepONet and the StablePDENet, and compare their solutions with the numerical solutions. As shown in the Table 8, the relative loss for PIDDeepONet is 0.0294, while the relative loss for StableNet is 0.0327. This shows that our method significantly outperform the PIDDeepONet. Using Figure 8 as an example, it also shows that the StablePDENet significantly outperforms the PIDDeepONet on the perturbed data.

Relative L^2 error w.r.t. true solution		
Network	Data	Relative L^2 error
PIDDeepONet	Original data	0.029
StablePDENet	Original data	0.031
PIDDeepONet	Attacked data	0.752
StablePDENet	Attacked data	0.036

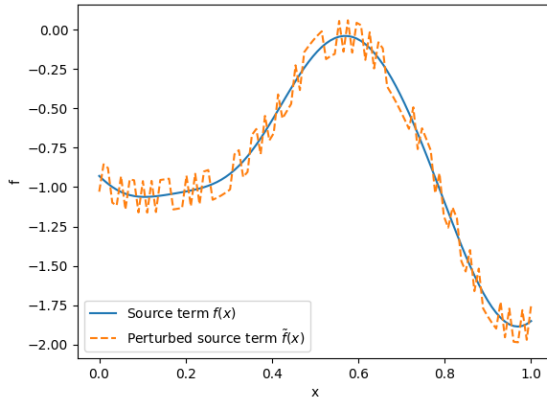
Table 8: Diffusion reaction equation

4.5.2 Diffusion Reaction Equation with coefficient perturbed

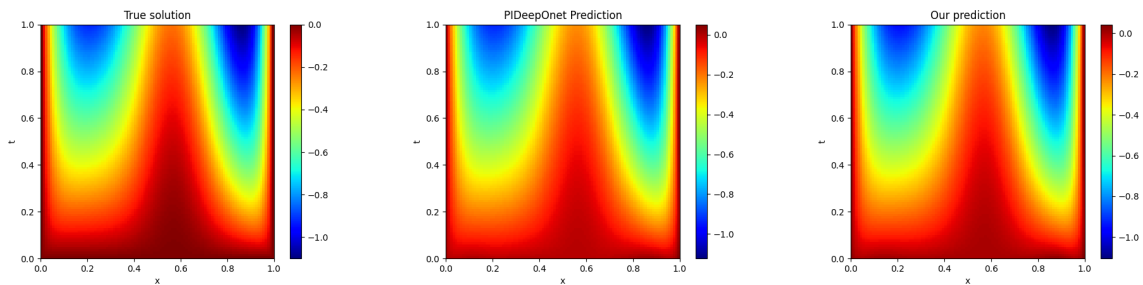
$$\frac{\partial u(x, t)}{\partial t} - D \frac{\partial^2 u(x, t)}{\partial x^2} + k(x) u^2(x, t) - f(x) = 0, \quad x \in [0, 1], t \in [0, 1]. \quad (24)$$

The boundary condition is the homogeneous Dirichlet boundary condition, and the initial condition is also the zero condition. $D = 0.01$, $f(x) = \sin(\pi x)$, we aim to learn a map from $k(x)$ to solution $u(x, t)$. Let $k(x)$ be generated from a Gaussian random field with length scale $l = 1.4$, and then scale the function to $[1, 5]$ to ensure the existence of the solutions. The other parameter settings for this experiment are the same as those in the previous experiment.

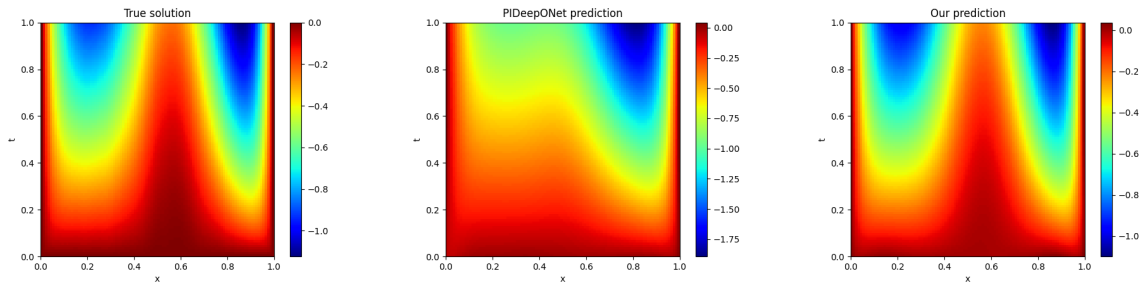
The error statistics are shown in Table 9, and the absolute errors of the PIDDeepONet and our method with respect to the numerical solution are shown in Figure 9. The results show both for the original source term and for their adversarially perturbed counterparts, our method achieve higher accuracy than PIDDeepONet for unperturbed inputs.



(a)



(b)

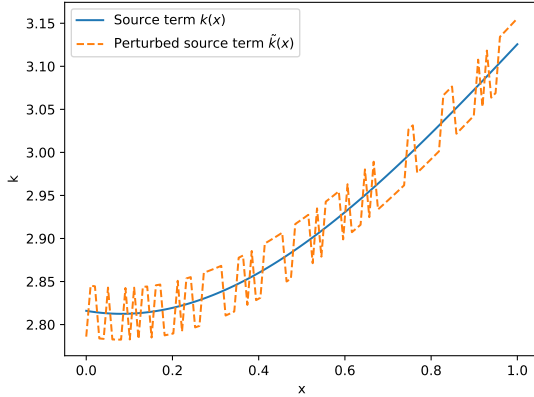


(c)

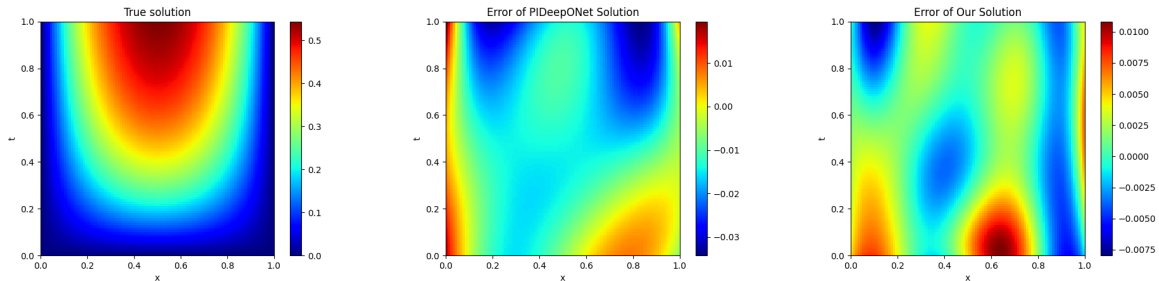
Figure 8: Solving diffusion reaction equation: one example. (a)The original source term and the perturbed source term; (b)Solutions w.r.t. the original source term; (c)Solutions w.r.t. the perturbed source term.

Relative L^2 error w.r.t. true solution		
Network	Data	Relative L^2 error
PIDeepONet	Original data	0.061
StablePDENet	Original data	0.017
PIDeepONet	Attacked data	0.10
StablePDENet	Attacked data	0.017

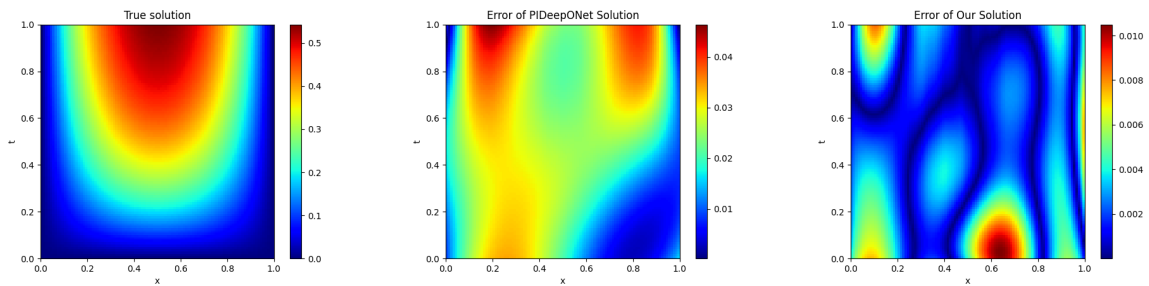
Table 9: Diffusion reaction equation with coefficient perturbed



(a)



(b)



(c)

Figure 9: Solving diffusion reaction equation with coefficient perturbed: (a)The original source term and the perturbed source term; (b)Absolute error w.r.t. the original source term; (c)Absolute error w.r.t. the perturbed source term.

4.6 Stokes Equation with Boundary Condition Perturbed

In this example, we use a PIDDeepONet to approach the system of Stokes for fluids. The domain is a 2D square full of liquid, with its lid moving horizontally at a given variable speed. The full equations and boundary conditions are

$$\begin{aligned}
& \mu \Delta u - \partial_x p = 0, \quad (x, y) \in (0, 1)^2 \\
& \mu \Delta v - \partial_y p = 0, \quad (x, y) \in (0, 1)^2 \\
& \partial_x u + \partial_y v = 0, \quad (x, y) \in (0, 1)^2 \\
& u(x, 1) = u_1(x), v(x, 1) = 0, \quad x \in (0, 1) \\
& u(x, 0) = v(x, 0) = p(x, 0) = 0, \quad x \in (0, 1) \\
& u(0, y) = v(0, y) = u(1, y) = v(1, y) = 0, \quad y \in (0, 1)
\end{aligned} \tag{25}$$

where u, v are the horizontal and vertical velocities, and p is the pressure. We attempt to learn an operator mapping from the boundary condition $u_1(x)$ to the solutions $\{u, v, p\}$, with $u_1(x)$ sampled from a Gaussian process with a radial basis function kernel of parameter $l = 0.2$. In addition, we multiply $u_1(x)$ by the factor $x*(1-x)$ in order to satisfy the compatibility boundary conditions.

We selected two perturbation parameters $\varepsilon = 0.1, 0.5$ for comparison. The error statistics the PIDDeepONet and the StablePDENet with respect to the numerical solution are shown in Table 10. The results show both for the original source term and for their adversarially perturbed counterparts, our method achieve higher accuracy than PIDDeepONet for unperturbed inputs. And the absolute errors of the StablePDENet for the two different perturbation scenarios are shown in Figure 10. The result indicates that as the perturbation magnitude increases, the advantage of our model becomes more pronounced. This further highlights the stability of the StablePDENet across varying perturbation levels.

Relative l2 error w.r.t. true solution				
Network	Data	u	v	p
PIDDeepONet	Original data	0.114	0.133	0.324
StablePDENet	Original data	0.086	0.010	0.304
PIDDeepONet for $\varepsilon = 0.1$	Attacked data	0.194	0.148	0.339
StablePDENet for $\varepsilon = 0.1$	Attacked data	0.090	0.101	0.305
PIDDeepONet for $\varepsilon = 0.5$	Attacked data	1.264	0.187	0.363
StablePDENet for $\varepsilon = 0.5$	Attacked data	0.110	0.108	0.333

Table 10: Stokes equation with boundary condition perturbed

4.7 Comparision of Jacobian Norm

To valid that the StablePDENet can control the norm of Fréchet derivative, we compare the results of our method with those of PIDDeepONet on both original data and attacked data. Specifically, we employ automatic differentiation technique to compute the Fréchet derivative, from which the Jacobian is obtained. The spectral norm of the matrix is used as approximation of the norm of Fréchet derivative. The results of all corresponding experiments are summarized in the Table 11.

The results indicate that the spectral norm of PIDDeepONet is consistently larger than that of StablePDENet, both on original and attacked data. This demonstrates the ability of our method to enforce a bound on the spectral norm, which implicitly guarantees the stability of the network. Notice that although the difference is less pronounced for experiment 4.2.2, the StablePDENet

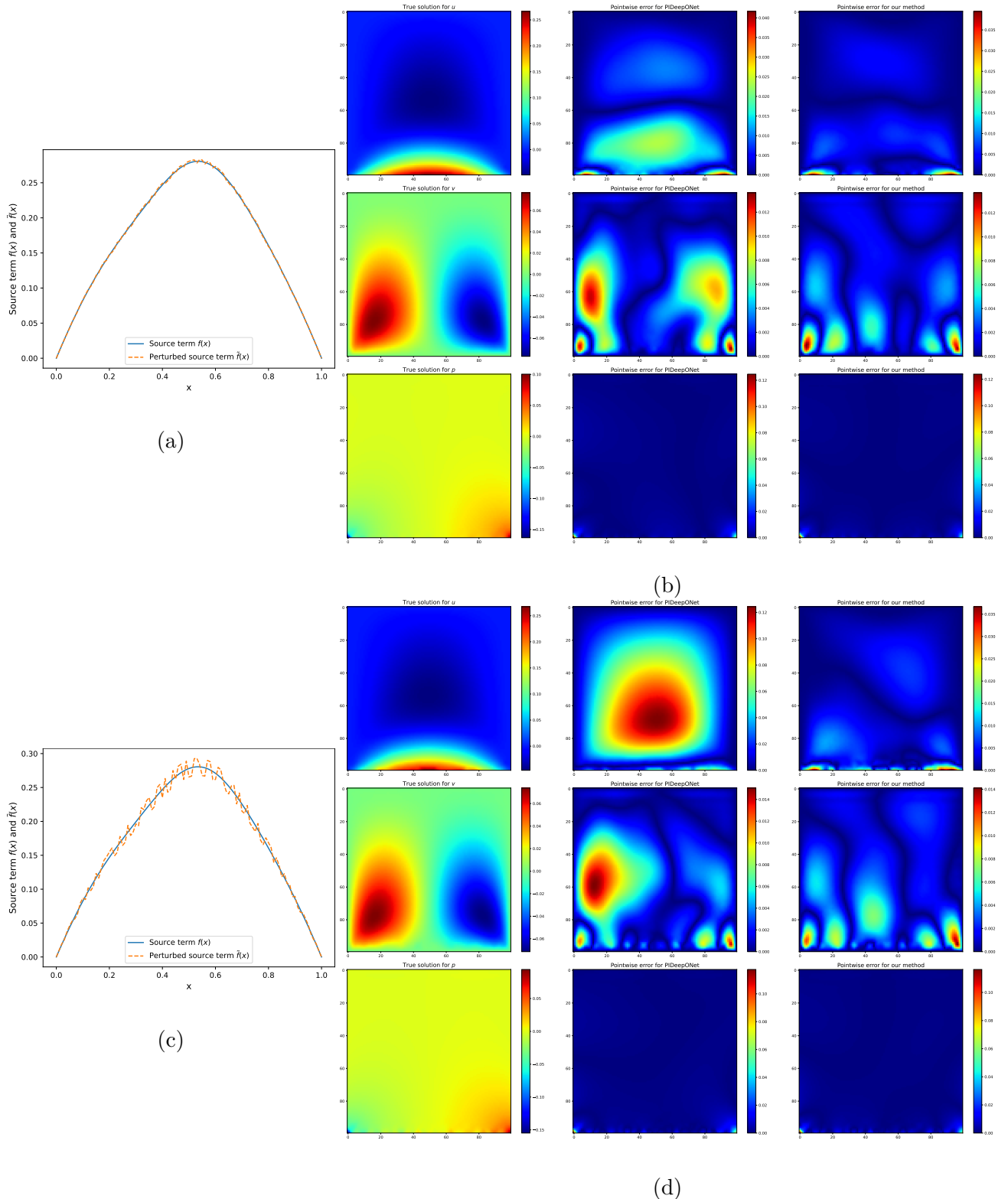


Figure 10: Solving Stokes equation for small perturbation. (a) The original source term and the perturbed source term with $\varepsilon = 0.1$; (b) Solutions w.r.t. the perturbed source term with $\varepsilon = 0.1$; (c) The original source term and the perturbed source term with $\varepsilon = 0.5$; (d) Solutions w.r.t. the perturbed source term with $\varepsilon = 0.5$.

Experiments	Original data		Attacked Data	
	PIDeepONet	StablePDENet	PIDeepONet	tablePDENet
4.1	3.966	1.058	3.940	1.052
4.2.1	27.699	0.293	27.228	0.296
4.2.2	0.009	0.008	0.008	0.008
4.3	5.845	0.806	5.217	0.806
4.4.1	14.030	1.916	12.144	1.900
4.4.2	1.479	0.241	1.440	0.240
4.5.1	1.747	0.262	1.673	0.257
4.5.2	0.751	0.251	0.728	0.248
4.6	0.051	0.011	0.052	0.011

Table 11: Comparision of Spectral Norm between StablePDENet and PIDeepONet.

still achieves significantly higher test accuracy than PIDeepONet on perturbed data, as shown in Table 4. In summary, the StablePDENet proves effective for stability of operator learning. In other words, our method enables networks to learn the derivatives of operators.

5 Conclusion

In this work, we present a stable framework named StablePDENet for learning solution operators of differential equations that maintain accuracy while significantly improving stability against input perturbations. The key innovation lies in our adversarial training paradigm, which systematically exposes the neural operator to worst-case input variations during training. The effectiveness of our method has been rigorously validated through comprehensive experiments, proving that our method not only preserves the accuracy of conventional methods on unperturbed inputs, but also demonstrates remarkable resilience to adversarial distortions. The demonstrated improvements in robustness suggest promising potential for deploying neural operators in real-world applications where input uncertainties and measurement noise are inevitable. This work represents an important step toward developing reliable, physics-aware machine learning methods for scientific computing.

Acknowledgement

The work was supported in part by the National Key Research and Development Program of China (No. 2025YFA1016800) and the Project of Hetao Shenzhen-HKUST Innovation Cooperation Zone HZQB-KCZYB-2020083.

Appendix A: Attack Algorithm to Generate Evaluation Data

In order to evaluate the performance of the models, we use the following algorithm to generate \tilde{f} from (f, u_{true}) , as described in Section 4.

Algorithm A1 Projected Gradient Descent Attack

Require: Input function f , coordinates y , pretrained model G_θ ;
Require: Attack parameters: step size α , perturbation bound ε , iterations n_{iter} ;

Initialize $\tilde{f}^{(0)} \leftarrow f$;
for $i = 0$ to $n_{\text{iter}} - 1$ **do**
 Forward pass: Compute $G_\theta(\tilde{f}^{(i)}, y)$
 Loss calculation: $\mathcal{L}^{(i)} \leftarrow \|G_\theta(\tilde{f}^{(i)}, y) - u_{\text{true}}(y)\|_2^2$
 Gradient computation: $g^{(i)} \leftarrow \nabla_{\tilde{f}} \mathcal{L}^{(i)}$
 Update perturbation: $\tilde{f}^{(i+1)} \leftarrow \tilde{f}^{(i)} + \alpha \cdot \text{sign}(g^{(i)})$
 Projection: $\tilde{f}^{(i+1)} \leftarrow \text{Clip}(\tilde{f}^{(i+1)}, f - \varepsilon, f + \varepsilon)$
end for
return $\tilde{f}^{(n_{\text{iter}})}$

The sign denotes the sign function, n_{iter} is the total iterations for PGD attacks, ε is the perturbation size allowed, and α is the step size.

References

- [1] Steven L Brunton, Bernd R Noack, and Petros Koumoutsakos. Machine learning for fluid mechanics. *Annual review of fluid mechanics*, 52(1):477–508, 2020.
- [2] Linfeng Zhang, Jiequn Han, Han Wang, Roberto Car, and Weinan E. Deep potential molecular dynamics: a scalable model with the accuracy of quantum mechanics. *Physical review letters*, 120(14):143001, 2018.
- [3] Gang Bao, Chang Ma, and Yuxuan Gong. PFWNN: a deep learning method for solving forward and inverse problems of Phase-Field models. *Journal of Computational Physics*, 527:113799, 2025.
- [4] Karthik Kashinath, M Mustafa, Adrian Albert, JL Wu, C Jiang, Soheil Esmaeilzadeh, Kamayyar Azizzadenesheli, R Wang, Ashesh Chattopadhyay, Aakanksha Singh, et al. Physics-informed machine learning: case studies for weather and climate modelling. *Philosophical Transactions of the Royal Society A*, 379(2194):20200093, 2021.
- [5] Yuyao Chen, Lu Lu, George Em Karniadakis, and Luca Dal Negro. Physics-informed neural networks for inverse problems in nano-optics and metamaterials. *Opt. Express*, 28(8):11618–11633, Apr 2020.
- [6] M. Raissi, P. Perdikaris, and G.E. Karniadakis. Physics-informed neural networks: A deep learning framework for solving forward and inverse problems involving nonlinear partial differential equations. *Journal of Computational Physics*, 378:686–707, 2019.
- [7] Weinan E and Bing Yu. The deep Ritz method: a deep learning-based numerical algorithm for solving variational problems. *Communications in Mathematics and Statistics*, 6(1):1–12, 2018.
- [8] Yaohua Zang, Gang Bao, Xiaojing Ye, and Haomin Zhou. Weak adversarial networks for high-dimensional partial differential equations. *Journal of Computational Physics*, 411:109409, 2020.

- [9] Lu Lu, Pengzhan Jin, Guofei Pang, Zhongqiang Zhang, and George Em Karniadakis. Learning nonlinear operators via deeponet based on the universal approximation theorem of operators. *Nature Machine Intelligence*, 3(3):218–229, 2021.
- [10] Zongyi Li, Nikola Borislavov Kovachki, Kamyar Azizzadenesheli, Burigede liu, Kaushik Bhattacharya, Andrew Stuart, and Anima Anandkumar. Fourier neural operator for parametric partial differential equations. In *International Conference on Learning Representations*, 2021.
- [11] Gordon D Smith. *Numerical solution of partial differential equations: finite difference methods*. Oxford university press, 1985.
- [12] Claes Johnson. *Numerical solution of partial differential equations by the finite element method*. Courier Corporation, 2009.
- [13] Peter D Lax and Robert D Richtmyer. Survey of the stability of linear finite difference equations. In *Selected Papers Volume I*, pages 125–151. Springer, 2005.
- [14] Dinshaw S Balsara. Von neumann stability analysis of smoothed particle hydrodynamics—suggestions for optimal algorithms. *Journal of Computational Physics*, 121(2):357–372, 1995.
- [15] Nicholas J Higham. *Accuracy and stability of numerical algorithms*. SIAM, 2002.
- [16] Arieh Iserles. *A first course in the numerical analysis of differential equations*. Number 44. Cambridge university press, 2009.
- [17] Keith W Morton and David Francis Mayers. *Numerical solution of partial differential equations: an introduction*. Cambridge university press, 2005.
- [18] Apostolos F. Psaros, Xuhui Meng, Zongren Zou, Ling Guo, and George Em Karniadakis. Uncertainty quantification in scientific machine learning: Methods, metrics, and comparisons. *Journal of Computational Physics*, 477:111902, 2023.
- [19] John Morris, Eli Lifland, Jin Yong Yoo, Jake Grigsby, Di Jin, and Yanjun Qi. Textattack: A framework for adversarial attacks, data augmentation, and adversarial training in nlp. In *Proceedings of the 2020 conference on empirical methods in natural language processing: System demonstrations*, pages 119–126, 2020.
- [20] Yao Deng, Xi Zheng, Tianyi Zhang, Chen Chen, Guannan Lou, and Miryung Kim. An analysis of adversarial attacks and defenses on autonomous driving models. In *2020 IEEE international conference on pervasive computing and communications (PerCom)*, pages 1–10. IEEE, 2020.
- [21] Mahmood Sharif, Sruti Bhagavatula, Lujo Bauer, and Michael K Reiter. Accessorize to a crime: Real and stealthy attacks on state-of-the-art face recognition. In *Proceedings of the 2016 ACM SIGSAC conference on computer and communications security*, pages 1528–1540, 2016.
- [22] Ian J. Goodfellow, Jonathon Shlens, and Christian Szegedy. Explaining and harnessing adversarial examples. *CoRR*, abs/1412.6572, 2014.
- [23] Aleksander Madry, Aleksandar Makelov, Ludwig Schmidt, Dimitris Tsipras, and Adrian Vladu. Towards deep learning models resistant to adversarial attacks. In *International Conference on Learning Representations*, 2018.

- [24] Kaibo Wang, Xiaowen Fu, Yuxuan Han, and Yang Xiang. Diffhammer: Rethinking the robustness of diffusion-based adversarial purification. *Advances in Neural Information Processing Systems*, 37:89535–89562, 2024.
- [25] Nicolas Papernot, Patrick McDaniel, Xi Wu, Somesh Jha, and Ananthram Swami. Distillation as a defense to adversarial perturbations against deep neural networks. In *2016 IEEE symposium on security and privacy (SP)*, pages 582–597. IEEE, 2016.
- [26] Aneesh Sreevallabh Chivukula, Xinghao Yang, Wei Liu, Tianqing Zhu, and Wanlei Zhou. Game theoretical adversarial deep learning with variational adversaries. *IEEE Transactions on Knowledge and Data Engineering*, 33(11):3568–3581, 2020.
- [27] Sifan Wang, Hanwen Wang, and Paris Perdikaris. Learning the solution operator of parametric partial differential equations with physics-informed deepnets. *Science advances*, 7(40):eabi8605, 2021.